DOI: 10.24996/ijs.2026.67.2.6

ISSN: 0067-2904

Synthesis, Characterization, and Elimination of Amoxicillin by Using V_2O_5 and NiO Nanoparticles

Ali. M. Jehad*, Rashed T. Rasheed

Chemistry Branch, Applied Science Department, University of Technology, Baghdad, Iraq

Received:7/1/2025 Accepted:3/9/2025 Published: xx

Abstract

The nanoparticles (V_2O_5 and NiO) were synthesized via reflux and characterized using various techniques including atomic force microscopy (AFM), scanning electron microscopy (SEM), X-ray diffraction (XRD), UV/visible spectroscopy, and Fourier-transform infrared spectroscopy (FTIR). Initially, the nanoparticles were dried at 90 ºC, to obtain the as prepared nanoparticles ($V_2O_5.1.8H_2O$ and $Ni(OH)_2$), followed by annealing at 500 ºC to produce the oxide nanoparticles (V_2O_5 and NiO). The average grain sizes of the nanoparticles as prepared were 30.51nm, 55.70 nm, which decreased to 21.49 nm and 37.07 nm after annealing, respectively. The nanoparticles were employed for the removal of amoxicillin (AMX) as a contaminant in a water solution. $V_2O_5.1.8H_2O$ nanoparticles exhibited the most effective removal activity among all types of nanoparticles, with a percentage removal (%R) of 64.01% and a removal capacity (qt) of 5.89 g/mg. Therefore, vanadium pentoxide in its prepared form ($V_2O_5.1.8H_2O$) demonstrated the best removal activity.

Keywords: nanoparticles, amoxicillin, V_2O_5, NiO, removal.

تحضير وتوصيف وإزالة الأموكسيسيلين باستخدام الجسيمات النانوية V_2O_5 وNiO

علي محمد جهاد* , راشد رشيد

قسم الكيمياء, الجامعة التكنولوجية, الجامعة,بغداد, العراق

الخلاصة

تم إنتاج المواد النانوية V_2O_5 و NiO عن طريق الارتجاع وتحليلها باستخدام تقنيات مختلفة مثل مجهر القوة الذرية(AFM) ، والمجهر الإلكتروني الماسح(SEM) ، وحيود الأشعة السينية(XRD) ، والتحليل الطيفي للأشعة فوق البنفسجية/المرئية، والأشعة تحت الحمراء لتحويل فورييه. التحليل الطيفي (FTIR). خضعت المواد النانوية لعملية تجفيف عند درجة حرارة 90 درجة مئوية، يليها التلدين عند درجة حرارة 500 درجة مئوية من أجل إنتاج جسيمات الأوكسيد النانوية V_2O_5 وNiO. وكان متوسط أحجام الحبوب للجسيمات النانوية 30.51 نانومتر، 55.70 نانومتر، 21.49 نانومتر، و 37.07 نانومتر لـ V_2O_5 و NiO على التوالي. تم استخدام الجسيمات النانوية لإزالة الأموكسيسيلين (AMX) كملوث في محلول مائي. أظهر خامس أكسيد الفاناديوم نشاط الإزالة الأكثر فعالية بين جميع أنواع الجسيمات النانوية، مع نسبة إزالة (%R) تبلغ 64.01 وقدرة إزالة (qt) تبلغ 0.438. أظهر الشكل المُجهز لأوكسيد الفاناديوم V_2O_5 أفضل نشاط إزالة.

---

*Email: al19893311@gmail.com

1. Introduction

Pollution is one of the most pressing problems that contemporary societies face on a global scale. A thorough understanding of its types and effects on human and environmental health is crucial since it has a negative influence on every facet of life. The sustainability of life on Earth is seriously threatened by ongoing environmental contamination; thus, knowledge and comprehension of this issue are important [1]. Water contamination is a worldwide issue that impacts all nations, irrespective of their degree of development. It is estimated that over 80% of global wastewater is discharged untreated into the environment, significantly harming ecosystems, human health, and the global economy [2]. Various contaminants can cause these effects, including oxygen-depleting pollutants like organic debris from sewage and runoff from farms [3]. Amoxicillin, a widely used antibiotic, effectively treats a range of bacterial infections, including those affecting the ear, skin, respiratory system, and urinary tract. It works well against a variety of bacteria, such as those that cause ear, skin, respiratory, and urinary tract infections [4].

Various techniques have been employed to eradicate antibiotics from water and wastewater, including adsorption methods, which are typically utilised to remove organic compounds by employing appropriate adsorbents [5]. Hence, it is imperative to examine the mechanism of antibiotics elimination through the process of adsorption in studies focused on adsorption. Amoxicillin (AMX) has been detected in various aquatic environments such as effluents, hospital effluents, and river and seawater. The harmful effects of this substance on aquatic creatures have been recently documented [6]. Therefore, AMX was chosen as a representative of antibiotics in this work on antibiotic removal utilising a novel adsorbent. The objective of this study is to synthesise nanoparticles, specifically vanadium pentoxide and nickel oxide nanoparticles, and study these nanoparticles for the removal of amoxicillin from aqueous solutions and their optimum conditions [7].

2. Materials and Methods

All chemical reagents used in this study were of high purity and required no further purification. Ammonium metavanadat (NH_4VO_3) with 99.9% was obtained from Sigma-Aldrich, while cetyltrimethyl ammonium bromide (CTAB) with 99.0%, was sourced from BDH, $[(C_{16}H_{33})N(CH_3)_3]$ Br. The hydrochloric acid (37%) and the urea (98.7%), potassium permanganate (99.7%), sodium hydroxide (99.0%), amoxicillin ($C_{16}H_{19}N_3O_5S$), (95%) from Samara Drug industry were used in the experiments. Moreover, nitric acid (HNO_3), (98%) from Alpha Chem was used. The ethanols (97%) from Sigma-Aldrich, ammonium hydroxide (99.9%) from Fluka, and Samara Drug Industry were utilized. The hydrogen peroxide (98%) from BDH was utilized.

The following equipment was utilized: A Sartorius (Germany) sensitive electric balance; a Jasco (India) magnetic stirrer; an FL 701383 (USA) shaker; a locally manufactured autoclave; an MSE (England) bench centrifuge; Gallenkamp (Germany) oven and furnace; Jenway (Germany) pH indicator and litmus test paper strip rolls. Fourier-transform infrared (FTIR) spectroscopy was performed using KBr discs on a Shimadzu FTIR-8400S spectrometer (4000-400 cm^{-1}). UV/Visible spectra were acquired using both a Shimadzu 1650 PC double-beam spectrophotometer and a UV-1100 (England) single-beam spectrophotometer. Scanning electron microscopy (SEM) employed a TESCAN VEGA microscope operating at 30kV with 10,000× magnification. Atomic force microscopy (AFM) was conducted using an SPM-AA 3000 instrument. X-ray diffraction (XRD) analysis was also performed.

3. Results and discussion

3.1. Synthesis of Vanadium Pentoxide Nanoparticles (V_2O_5).

Vanadium pentoxide (V_2O_5) was synthesised using the hydrothermal method [8]. Concentrated nitric acid (HNO_3), cetyltrimethylammonium bromide (CTAB), and ammonium metavanadate (NH_4VO_3) were employed in the process. Specifically, 2 g (1.704 mmol) of NH_4VO_3 and 0.2 g (0.548 mmol) of CTAB were dissolved, respectively. Nitric acid was then added dropwise while stirring until the pH was adjusted to 2.5. The mixture was then heated and refluxed for six hours. After removing contaminants, the sediment product is repeatedly cleaned in distilled water, as indicated in equations 1 to 3, dried for 60 minutes at 90°C, and subsequently annealed for 120 minutes at °C.

$$2NH_4VO_3 + 2HNO_3 + nH_2O \xrightarrow[CTAB]{CH3CH2OH} V_2O_5nH_2O + 2NH_4NO_3 + (n-1)H_2O \quad (1)$$

$$V_2O_5.nH_2O \; 90°C \rightarrow V_2O_5.1.8\,H_2O + (n-1.8)H_2O \quad (2)$$

$$V_2O_5.1.8\,H_2O \; 500°C \rightarrow V_2O_5 + 1.8\,H_2O \quad (3)$$

3.2. Synthesis of Nickel oxide Nanoparticles (NiO NPs)

Nickel oxide nanoparticles (NiO) were synthesised using Sol-gel methods, following the procedure outlined in reference [9], which differs from the synthesis of V_2O_5. The sol-gel technique is widely employed to produce different nanostructures and metal oxide nanoparticles, while the hydrothermal method is a solution-based approach in nanotechnology for producing nanomaterials. The synthesis was performed with some modifications utilizing ammonium hydroxide (NH_4OH), cetyltrimethylammonium bromide (CTAB), and nickel ($NiCl_2.6H_2O$). The utilisation of CTAB in this sol-gel technique results in the production of NiO nanoparticles with reduced agglomeration. First, 3g (mmol) of $NiCl_2.6H_2O$ was dissolved in 200ml of distilled water. Next, it was mixed with 0.2g (mmol) of CTAB, which was dissolved in distilled water and added to it. Finally, 3ml of NH_4OH was diluted in 27ml of distilled water, and titrated with the final solution (mixture of CTAB and nickel chloride) using a magnetic stirrer until the reaction was finished, converting to a blue precipitate that was repeatedly washed with distilled water.

Subsequently, the precipitate was dried at 90°C for 60 minutes and then annealed at 500°C for 120 minutes.

$$NiCl_2.\,6H_2O + 2NH_4OH \; 90°C \rightarrow Ni(OH)_2 + 2NH_4Cl + 6\,H_2O \quad (4)$$

$$Ni(OH)_2 \; 500°C \rightarrow NiO + H_2O \quad (5)$$

3.3. Adsorption of amoxicillin (AMX) pollutant

The nanoparticles ($V_2O_5.1.8H_2O$, $Ni(OH)_2$), along with their annealing samples (V_2O_5, NiO,) were used for the adsorption of amoxicillin from an aqueous solution. Adsorption experiments were performed following the procedure described in reference [10]. Moreover, the concentration of AMX solution is 9.654×10^{-4} M, concentration of $KMnO_4$ is 8.033×10^{-3} M.

3.4. Consequences

3.4.1. Optical characteristics of nanoparticles.

A Shimadzu 1650 PC dual-beam UV-Vis spectrophotometer was employed to record the optical absorption spectra of the materials. The ethanol-dispersed nanoparticle solutions display optical characteristics between 250 and 800 nm in wavelength. As illustrated in Figure 1, the band gap at two different temperatures (90°C and 500°C) can be determined by plotting optical transmission versus wavelength. The values were calculated and used. To find the size of the energy gap, use the following equation:

$$Energy\ gap\ (eV) = 1240/\lambda\max \qquad (6)$$

The symbol λmax represents the wavelength at which the first maximum transmittance occurs. The factor 1240 is utilised to convert the unit of wavelength from nanometers (nm) to electron volts (eV). Figure 1-a, depicts the phenomenon of red shift in the transmittance edge, where the wavelength at which it occurs has grown from 383 nm (3.23 eV) for $V_2O_5.1.8H_2O$ to 520 nm (2.38 eV) for V_2O_5, when the annealing temperatures were raised to 500 °C. This finding is consistent with the reference [11]. The spectrum of $Ni(OH)_2$, as shown in Figure 1-b, has undergone a red shift, moving to a higher wavelength. Specifically, it has shifted from 244 nm (5.08 eV) to 500 nm (2.48 eV) for NiO, as indicated by equation 6. These results are consistent with the findings reported in reference [12]. The increased optical transmittance can be attributed to the homogeneity of the structure and the crystallisation of particles.

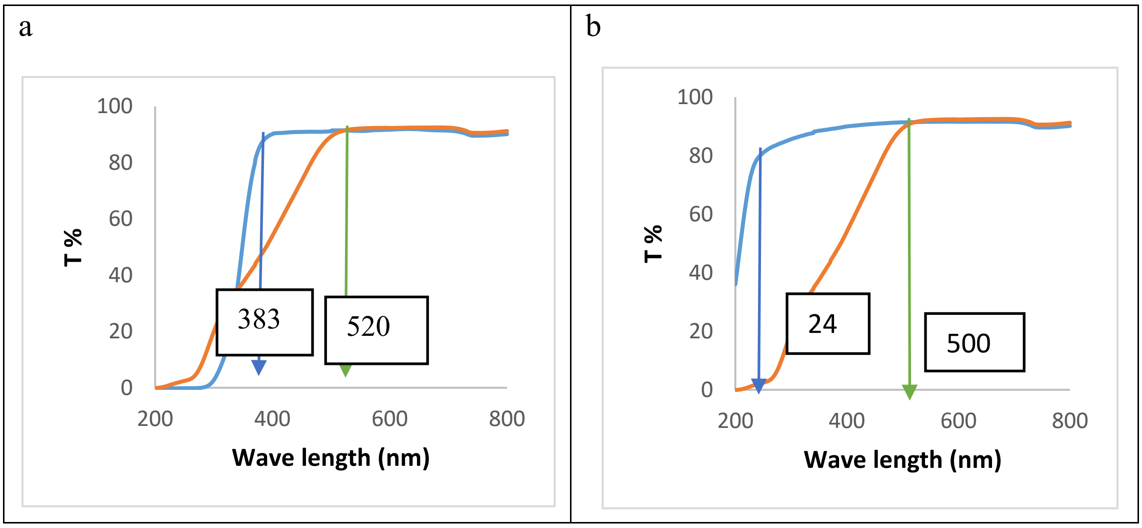

Figure 1: Nanoparticle optical transmittance (a: V_2O_5, b: NiO after annealing at 90 °C and 500 °C, respectively. Shades of blue when prepared and crimson when annealed.

3.4.2. The FTIR spectrum

FTIR is a valuable technique for identifying the functional groups involved in the synthesis of metal oxide synthesis is (FTIR). The nanoparticles were synthesised using KBr discs in the 400 cm^{-1} to 4000 cm^{-1} wavenumber range.

3.4.2.1. FTIR Spectra for $V_2O_5.1.8H_2O$ and V_2O_5 nanoparticles

Figure 2-a shows O-H stretching and bending vibrations are visible in the Fourier Transform Infrared (FTIR) spectra of $V_2O_5.1.8H_2O$ nanoparticles (in their original state) after 60 minutes of heating at 90 °C. A broad band at 3205 cm^{-1} and a prominent peak at 1655 cm^{-1} indicate these vibrations, respectively. The carbon-carbon double bond (C=C) in CTAB is responsible for the bending vibration, which is reflected at 1410 cm^{-1}. Wavenumbers 966 cm^{-1}, 729 cm^{-1}, and 524 cm^{-1} are characterized by the peaks of vanadium pentoxide ($V_2O_5.1.8H_2O$) nanoparticles. V=O, V-O-V symmetric, and V-O-V asymmetric modes correspond to the vibrations of these peaks, respectively. As a bonus, a peak at 405 cm^{-1} is seen for V-O stretching [13].

Figure 2-b shows the V_2O_5 annealing procedure, which consists of heating the material to 500 °C for 120 minutes. The frequency of the stretching vibration of V=O is 1020 cm^{-1}, while the frequency of the deformation mode of V-O-V is 823 cm^{-1}. Bands at 597-476 cm^{-1} are associated with the stretching vibrations of V-O-V and V-O bonds in V_2O_5 coordination [14].

3.4.2.2. FTIR Spectra for Ni (OH)$_2$ and NiO nanoparticles

In Figure 2-C, it can be observed that a peak at 3637 cm^{-1} is observed in the Fourier transform infrared (FTIR) spectra of $Ni(OH)_2$ nanoparticles, which is attributed to the stretching of O-H bonds [15]. Wavenumbers 522 to 454 cm^{-1} are the most intense for the Ni-O bond. Figure 2-D shows the Fourier transform infrared spectra of the nickel oxide sample that was annealed at 500 °C. The broad spectral bands seen in Figure 2d between 1514 and 1016 cm^{-1} are explained by the stretching of C=O and the bending vibrations of H-O-H. The stretching vibration of the O-C=O bond is correlated with the signal at 833 cm^{-1}. In addition, there is a peak at 511 cm^{-1} and the stretching vibration of the C-O bond at 624 cm^{-1}.

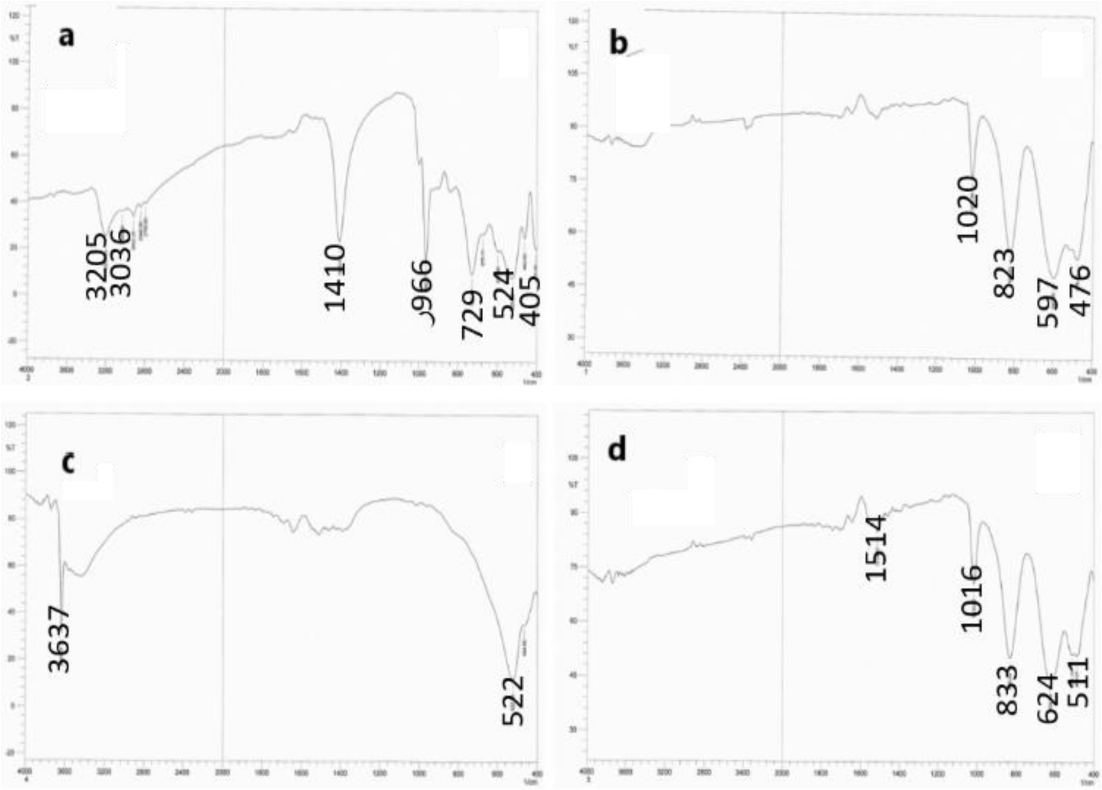

Figure 2: FTIR spectrum of (a)$V_2O_5.1.8H_2O$. (b) V_2O_5, (C) $Ni(OH)_2$, (d) NiO)

3.4.3. The X-Ray Diffraction for $V_2O_5.1.8H_2O$ and V_2O_5 nanoparticles

Figure 3 displays the X-ray diffraction (XRD) results for $V_2O_5.1.8H_2O$, a compound produced using the hydrothermal approach with reflexes at several temperatures, including as-prepared at 90 °C and annealed at 500 °C. The 2θ values of (11.299, 27.706, 30.642) correspond to the diffraction peaks of (002), (411), and (600), and are the most prominent primary peaks noticed. The major diffraction peaks of 2θ = (20.1987, 26.029, 30.891) are identified by the card number (JCPDS card No.01-089-0612) [17] and may be linked to $V_2O_5.1.8H_2O$. According to the standard diffraction pattern, the V_2O_5 planes (110), (100), and (002) exhibit diffraction peaks. According to the information on JCPDS card no. 41-1426, these peaks are in agreement with the V_2O_5 pattern. Lattice parameters of a = 11.569 °A, b = 3.580 °A, and c = 4.160 °A, indicate that the diffraction peaks are caused by an orthorhombic structure of the $V_2O_5.1.8H_2O$ phase [30]. It is possible to determine the particle sizes of the crystals by applying the Scherrer equation (7). The nanocrystal defined by this equation belongs to the orthorhombic system based on the acquired lattice constants. The Debye-Scherrer formula is widely used to estimate crystallite size from the FWHM of XRD diffraction peaks.

$$D=K\lambda/\beta cos\ \theta \tag{7}$$

The above equation depicts the connection between multiple parameters. The size of the crystallite is denoted by D, the shape factor is denoted by k, which has a value of 0.98, the X-ray wavelength is denoted by λ, and the line broadening at half-maximum intensity (FWHM) of an individual peak at 2θ (where θ is the Bragg angle) is denoted by γ [18]. The Scherer equation was used to find the average grain size of V_2O_5 nanoparticles. Table 1, and equation 8 were used to estimate the lattice constants (a), (b), and (c) of $V_2O_5.1.8H_2O$ and V_2O_5 nanoparticles, respectively.

$$1/d^{2}_{hkl}=h2/a2+k2/b2+I2/c2 \tag{8}$$

In this context, (d) stands for the distance parameter, (hkl) the Miller indices, and (a, b, c) the lattice constants. The XRD data for V_2O_5 at 90 °C for 60 min and at 500 °C for 120 min are shown in Table 1.

3.4.3.1. X-ray Diffraction for Ni $(OH)_2$ and NiO nanoparticles

At 2θ = (20.236, 26.108, 30.961) and 2 = (32.980°, 38.428°, 52.707°, 58.945° and 62.588°) that correspond to the diffraction planes (100, 101, 102, 110 and 001) respectively. Figure 3c. The lattice constant a= 3. 133 and c= 4.622 °A, (JCPDS number-04-0835), corresponding to the hexagonal wurtzite phase of $Ni(OH)_2$ nanoparticles, equation 9. And match those mentioned in the cited work [17]. Furthermore, apart from the typical NiO peaks, the XRD spectrum displayed other peaks. Annealing results at 500 °C (JCPDS card No. 44-1159) and it corresponds to a cubic structure with lattice constant a= 4.311°A [19]. Using the Scherrer equation 7, one can find the NiO nanoparticles' crystal particle size and their lattice constants equation 10. Figure 3d and Table 1 show how the Scherrer equation is applied.

$$1/\ d^{2}_{hkL}=4(h^{2}+hk+k^{2})/\ 3a^{2}+(\ I^{2}/C^{2}) \tag{9}$$

$$1/d^{2}_{hkl}=\frac{h^{2}+k^{2}+\ l^{2}}{a^{2}} \tag{10}$$

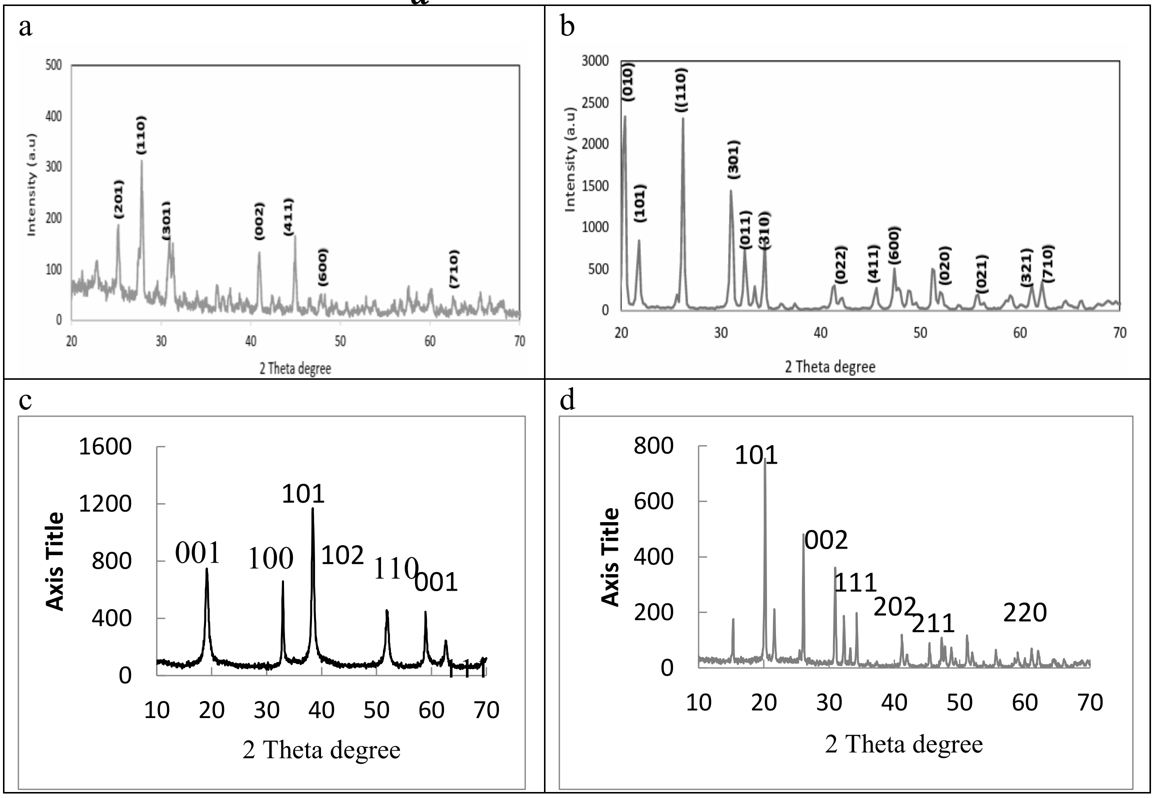

Figure 3: The XRD of(a) $V_2O_5.1.8H_2O$,(b) V_2O_5,(C) $Ni(OH)_2$,(d), NiO

Table 1 The XRD results of metal oxide heated at 90 ºC for 60 min and at 500 ºC for 120 min

	2θ	**hkL**	**FWHM**	**d**	**D**	**Lattice constant (A°)**		
	(deg)		**(deg)**	**(A°)**	**(A°)**	**a**	**b**	**c**
V_2O_5 1.8 H_2O	21.376	010	0.138	4.153	579.218	11.660	3.550	4.153
	27.706	110	0.169	3.217	477.231	-------	-------	-------
	30.642	400	0.204	2.915	399.187	-------	-------	-------
V_2O_5	20.198	010	0.248	3.420	321.209	11.569	3.700	4.153
	26.029	110	0.248	3.420	324.525	-------	-------	-------
	30.891	301	0.287	2.892	283.652	-------	-------	-------
Ni(OH)$_2$	38.42	001	0.475	2.340	175.446	3.133	4.622	------
	19.18	110	0.662	4.622	120.552	- ----	-----	…..
	32.98	200	0.344	2.713	238.905	-----		……
NiO	20.24	101	0.205	4.384	391.044	4.311	4.311	----
	26.11	100	0.183	3.410	441.573	- ----	----	…..
	30.96	002	0.221	2.885	370.754	- ----	----	……

3.4.4. Surface morphology

3.4.4.1. Vanadium pentoxide (V_2O_5) nanoparticles

Figures 4a and 4b display atomic force microscopy (AFM) images of V_2O_5 that were synthesised and subjected to different temperatures for annealing (90 °C and 500 °C). The findings indicate that the dispersion and accumulation of nanoparticles are initially observed as large balls (Figure 4a), However, during annealing at 500°C, their size decreases (Figure 4b). The following equation describes the process by which water molecules are removed from the sample, which is responsible for these results. Table 2 [18] demonstrates that when the temperature increases from 90 to 500°C, the average grain size decreases from 30.51 nm [V_2O_5.1.8H_2O] to 21.49 nm of V_2O_5, which is in agreement with the results obtained from AFM research.

3.4.4.2. Nickel oxide (NiO) nanoparticles

Figures 7a and 7b display atomic force microscopy (AFM) images of nickel oxide (NiO) nanoparticles. These nanoparticles were produced and annealed at different temperatures. The images show that the dispersion and accumulation of NiO nanoparticles change from an oval shape (Figure 4c) to the largest size (Figure 4d). This transformation is caused by the fact that when heated to 500°C, the majority of hydroxides (Ni(OH)$_2$) transform into oxides (NiO). The data in Table 3 support this trend. Furthermore, increasing temperature leads to a decrease in nanoparticle grain size, from 55.70 nm to 37.07 nm [19].

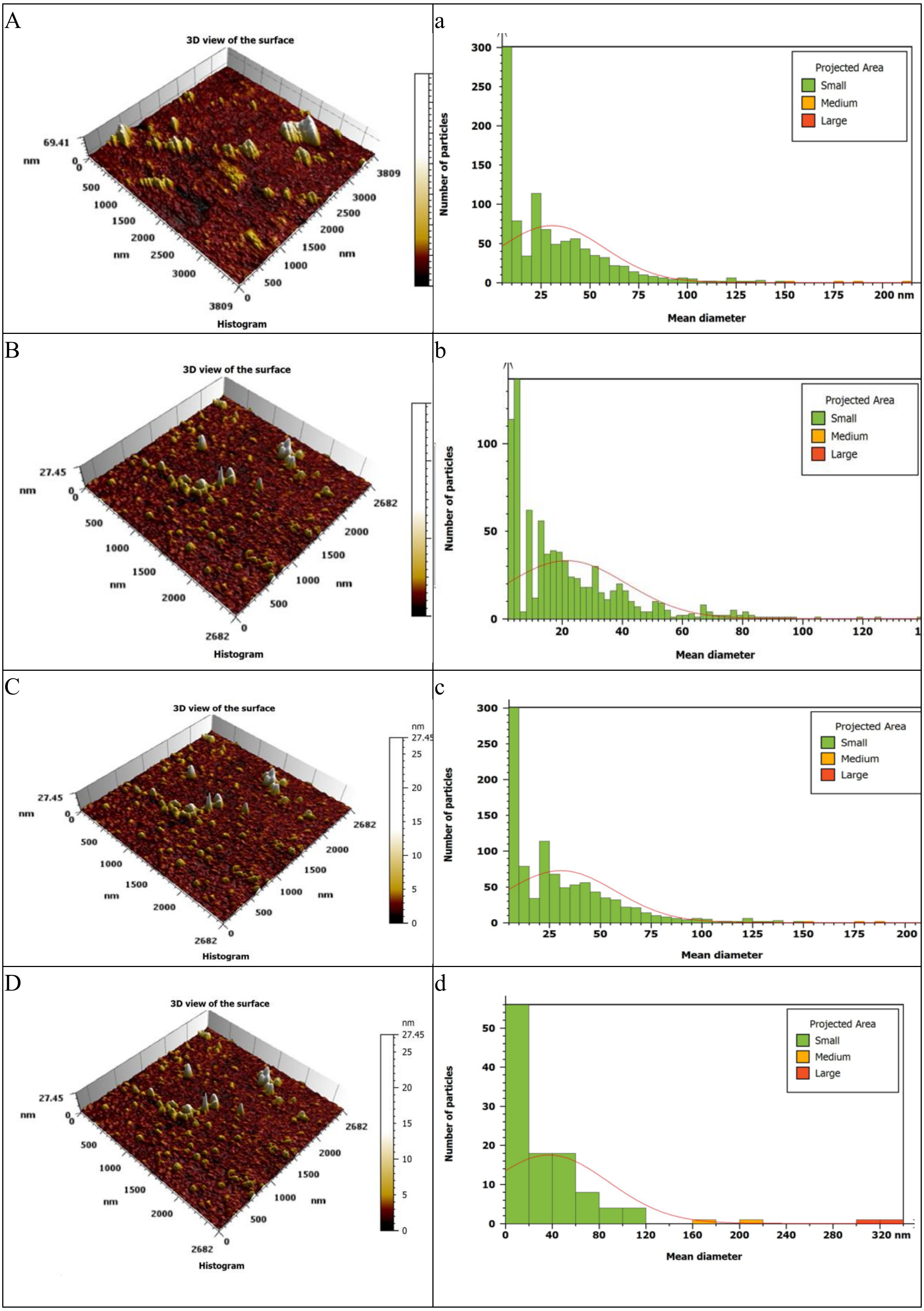

Figure 4: AFM images aT3D and Garsnularity accumulation distribution charts of (a) $V_2O_5.1.8H_2O$,(b) V_2O_5, (c) $Ni(OH)_2$, (d) NiO.

Table 2: Variation of grain Size for vanadium oxide and nickel oxide at 90℃ and 500 ℃ Average grain size (nm)

Sample	As-prepared (90 oC)	Annealing (500 ºC)
V_2O_5	30.51	21.49
NiO	55.70	37.07

3.4.5. Surface morphology by SEM

SEM was employed to investigate the morphology of the nanoparticles in the $V_2O_5\cdot1.8H_2O$ and $Ni(OH)_2$ samples. These samples were heated at 90°C for the initial 60 minutes of synthesis. In contrast, the (V_2O_5, NiO) samples, on the other hand, were annealed at 500 °C for 120 minutes. Figure 5a displays the results of the scanning electron microscopy (SEM) study, which was carried out at a 2 µm magnification. The surface of the samples showed a high porosity structure, which was further enhanced by raising the temperatures used for preparation and annealing, according to the data. Surface observations revealed nanoparticle clusters and clumps. Clusters are shown in Figure 5a, which is the scanning electron microscopy (SEM) picture of the unprocessed V_2O_5 nanoparticles. In contrast, NiO seems to have a cubical surface morphology (Figure 5b). SEM picture of the NiO particles shows a broad range of particle sizes and morphologies, including flaky and platelet-like particles [25]. The results from AFM are consistent with the SEM images, which reveal the material to be nanoclusters. V_2O_5, according to the AFM measurements, has the largest average grain size (21.49 nm) of all the oxide nanoparticles after annealing at 500°C.

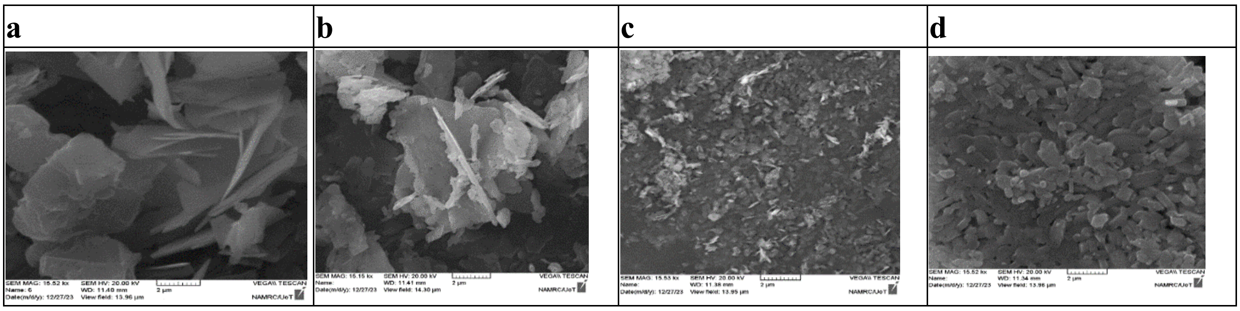

Figure 5: SEM image for (a) $V_2O_5.1.8H_2O$, (b) V_2O_5, (c) $Ni(OH)_2$, (d) NiO

4. Applications (Adsorption of Pollutants)

The produced nanoparticles, along with annealing, were examined for their ability to adsorb amoxicillin as a pollutant. The following methodologies were employed in the studies:

4.1. The Adsorption of AMX Pollutants

The percentage removal (%R) of amoxicillin varied based on the type of composite and its condition (either as prepared or annealed). The %R values for the nanoparticles were as follows: $V_2O_5.1.8H_2O$ > $Ni(OH)_2$. For the samples obtained in this experiment, the concentration of V_2O_5 is greater than that of NiO. Regarding the annealing of samples, the adsorption capacities (qt) of these samples followed the same order as they were prepared ($V_2O_5.1.8H_2O$ > $Ni(OH)_2$), and the opposite order (V_2O_5 > NiO) for annealed samples. This difference may be attributed to the V_2O_5 sample having the smallest grain size (21.49 nm), which results in the highest surface area for the adsorption of Amoxicillin, as depicted in Figure 6 and Table 3.

4.1.1. Optimum conditions

The nanoparticles $V_2O_5.1.8H_2O$ and $Ni(OH)_2$ were utilized to adsorb pollutants in two scenarios: as-prepared and under annealing conditions. Each nanoparticle, V_2O_5 and NiO, was prepared with a consistent weight (0.01 g) and volume (27 ml). The objective was to determine the most effective nanoparticle for removing the pollutants (AMX).

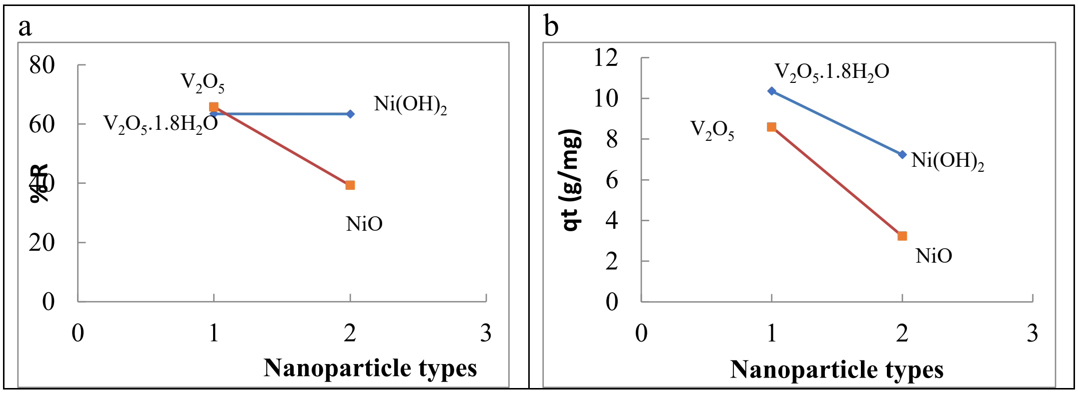

Figure 6: a: Percentage removal (%R), and b: adsorption capacity (qt) of Amoxicillin contamination on to nanoparticles.

Table 3: Percentage removal (%R) and adsorption capacity (qt) of Amoxicillin contamination on to nanoparticles.

Nano particles	percentage removal (% R)		Adsorption capacity (qt) mg/g	
	AS-prepared	**Annealing**	**AS-prepared**	**Annealing**
V_2O_5	64.10	60.91	8.76	8.56
NiO	60.09	58.93	8.08	8.04

4.1.1.1. Optimum condition of $V_2O_5.1.8H_2O$ of amoxicillin pollutants

Various parameters were examined to ascertain the optimal settings, including the starting nanoparticle weight, starting AMX concentration, the impact of shaking speed, and the impact of shake time.

A. Effect of weight

The effect of weight on AMX pollution clearance was studied by using $V_2O_5.1.8H_2O$ with different weights (0.01, 0.015, 0.020, 0.025, 0.030, and 0.035) g while keeping the AMX concentration constant at $9.654 X10^{-4}$ M. The experimental conditions comprised an alkaline $KMnO_4$ solution, shaking at 250 rpm for 15 minutes. Figure 7 and Table 4 provide a concise summary of the data within 15-minute time frame. The AMX removal percentage had a positive correlation with the weight of the sorbent ($V_2O_5.1.8H_2O$), but showed a negative correlation with increasing sorbent. The highest level of adsorption (58.96 %R, 0.266 qt) was achieved with a weight of 0.015 g, while the other variables were pollutants.

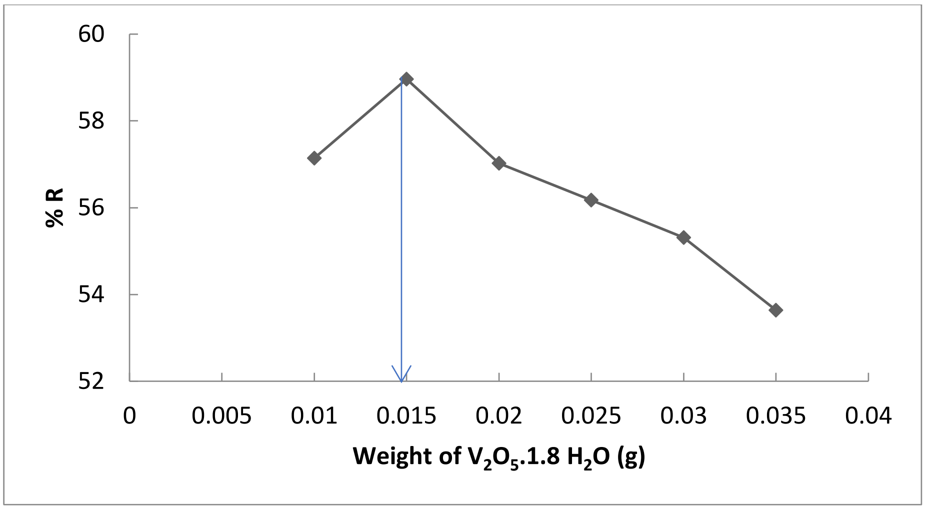

Figure 7: The effect of adsorbent weight on AMX removal.

Table 4: The relationship between the AMX pollutant and the percentage removal (%R) corresponding with the weight of nanoparticles.

	Weight (g)	**percentage removal (% R)**
$V_2O_5.1.8H_2O$	0.01	57.142
	0.015	58.964
	0.02	57.021
	0.025	57.142
	0.03	55.309
	0.035	53.636

B. Effect of AMX *concentration*

The elimination process was examined to determine the effect of different AMX concentrations. The following AMX concentrations were used: 3.75, 7.5, 11.25, 15.00, 18.75, 22.50, and 26.25 ppm, with a constant weight of 0.015 g of $V_2O_5.1.8H_2O$. The parameters for the shake were 250 rpm for the shaking speed, 15 minutes for the shake length, and 15 ppm for the AMX concentration. Table 5 and Figure 8 summarise the results. An increased concentration of AMX led to a faster elimination rate. Under constant conditions, the highest adsorption was observed at a concentration of 15 ppm, with measurements of 56.666 %R and 4.89 qt. The accumulation of several layers of the adsorbent (AMX) onto the nanoparticles could explain this behavior.

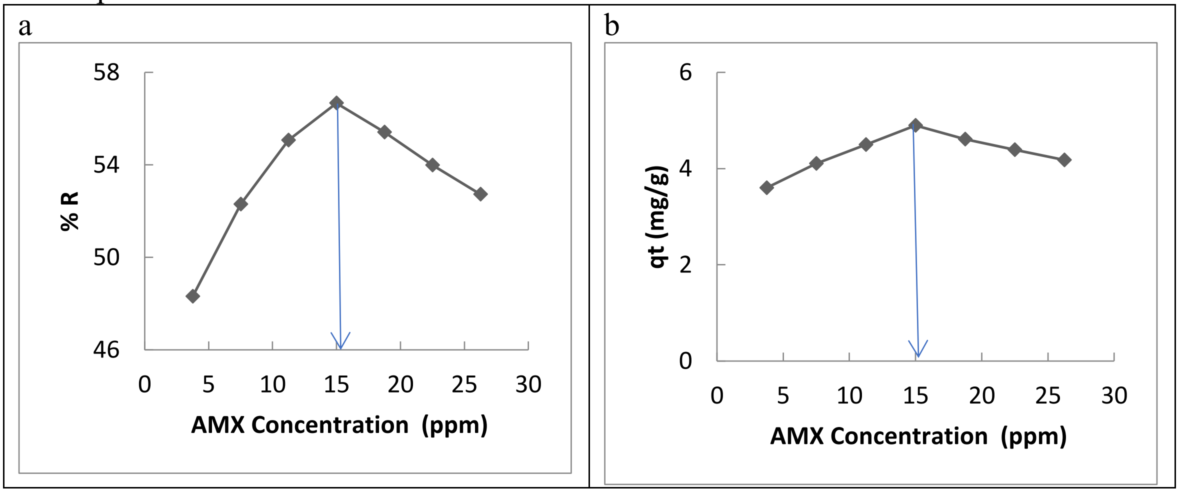

Figure 8: effect of concentration on the removal AMX.

Table 5: As a function of AMX concentration, the values of adsorption capacity (qt) and percentage removal (R%)

	Concentration (ppm)	Percentage removal (% R)	Adsorption capacity (qt(mg/g)
$V_2O_5.1.8H_2O$	3.75	48.309	3.60
	7.50	52.293	4.10
	11.25	55.066	4.50
	15.00	56.666	4.89
	18.75	55.411	4.60
	22.50	53.982	4.39
	26.25	52.727	4.17

C. Effect of $KMnO_4$ concentration

The elimination process was examined to determine the effect of different $KMnO_4$ concentrations. In particular, $KMnO_4$ concentrations of 28.24, 65.48, 84.72, 122.96, 141.20, 169.44, and 197.68 ppm were deployed. This experiment used the following variables: a pH level of 10, a shaking speed of 250 rpm, a duration of 15 minutes, a fixed weight of $V_2O_5.1.8H_2O$ (0.015 g), and an AMX concentration of 15 ppm. An abbreviated version of the results is presented in Table 6 and Figure 9. Removing $KMnO_4$ became more efficient as the concentration of $KMnO_4$ rose. A concentration of 122.96 ppm resulted in the maximum absorption (58.4%R, 5.11 qt) when all other factors remained constant. Nanoparticles may have been coated with many layers of adsorbent ($KMnO_4$), which could explain this behavior.

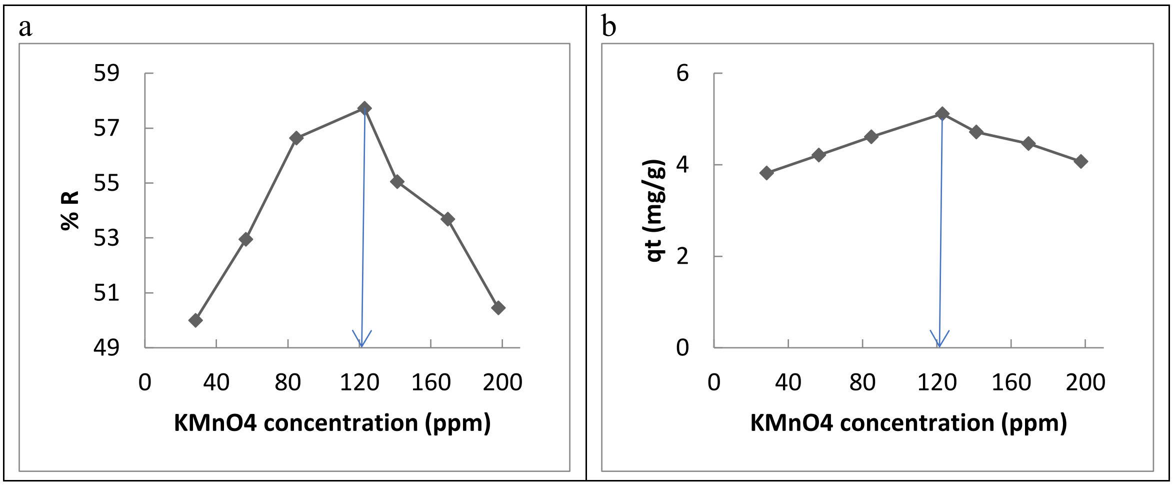

Figure 9: Effect of concentration on the removal of kmno4.

Table 6: The effect of kmno4 concentration on the values of adsorption capacity (qt) and percentage removal (R %)

	$KMnO_4$ concentration	Percentage removal (% R)	Adsorption capacity (qt)
$V_2O_5.1.8H_2O$	28.24	50.00	3.81
	56.48	52.94	4.21
	84.72	56.63	4.60
	122.96	57.72	5.11
	141.2	55.04	4.71
	169.44	53.67	4.46
	197.68	50.44	4.06

D. Effect of shake speed

Using a shake time of 15 minutes, a concentration of $KMnO_4$ (122.96 ppm), a weight of $V_2O_5.1.8H_2O$ kept constant at 0.015 g, and shake speeds of 50, 100, 150, 200, and 250 rpm, we examined the effect of shaking speed on AMX elimination. An abbreviated version of the results is presented in Table 7 and Figure 10. An inverse relationship between shaking speed and AMX elimination rate was observed. Setting all other parameters constant, the maximum adsorption level was measured at 250 rpm (65.68 %R, 6.40 qt). This is related to the relationship between the ramping up of velocities, which causes an increase in collision energy and, consequently, adsorption. Instabilities and declines in the adsorption of particles on nanoparticle surfaces occur at speeds greater than 250 rpm [23].

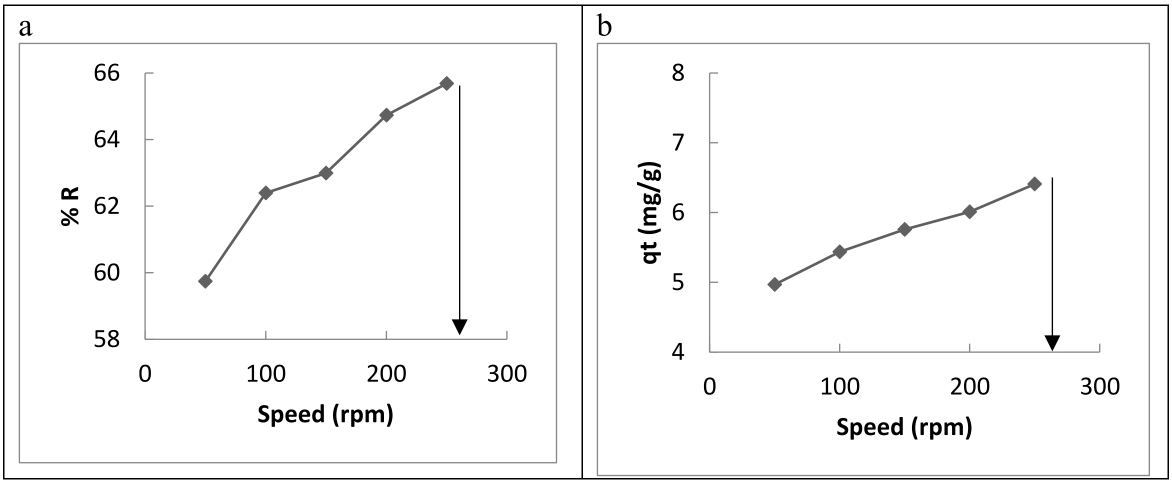

Figure 10: Effect of shake speed on AMX removal.

Table 7: Results for the effect of shaking speed on percentage removal (%R) and adsorption capacity (qt).

Shake speed	Percentage removal (% R)	Adsorption capacity (qt)mg/g
50	59.74	4.96
100	62.39	5.43
150	62.99	5.76
200	64.72	6.01
250	65.68	6.40

E. Effect of shake time

A constant weight of $V_2O_5.1.8H_2O$ (0.015 g), a concentration of AMX of 15 ppm, a basic solution of $KMnO_4$, a shake speed of 250 rpm, and different shaking times ranging from 10 to 70 minutes were used to assess the impact of shake time on the removal of AMX. A brief synopsis of the results reported in reference [23] is given in Figure 11 and Table 8. Maximal elimination percentage of 58.4%R and a value of 5.25 qt can be achieved by increasing the shaking period from 10 to 70 minutes. After 20 minutes, the optimal result is achieved. Beyond this point, the time required gradually decreases, ranging between twenty and seventy minutes. Particles dropping off nanoparticle surfaces as a consequence of higher particle collisions increase the shaking time, which in turn causes the effects [24].

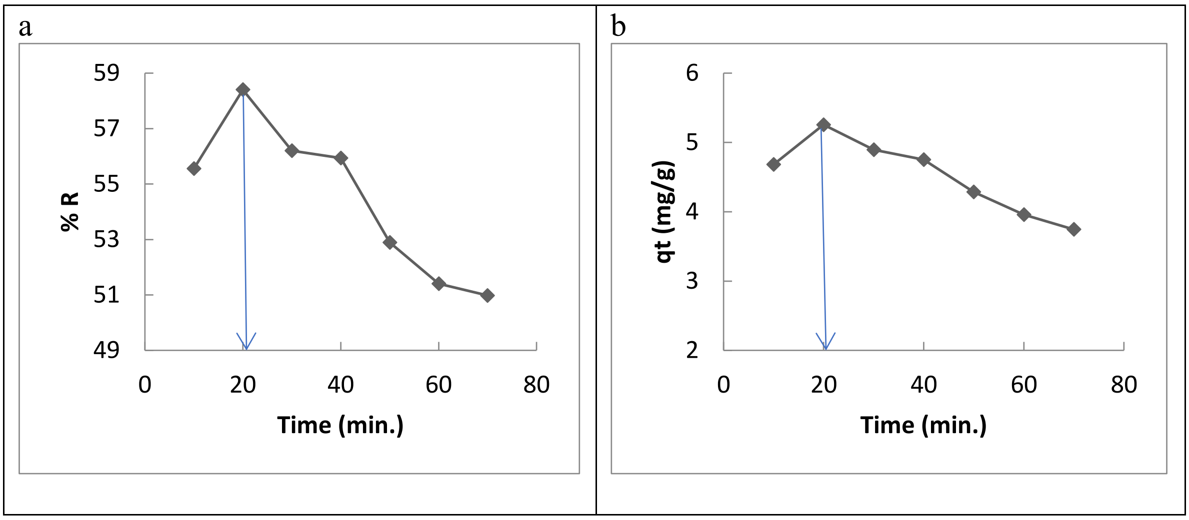

Figure 11: Effect of shake time on AMX removal.

Table 8: The values of (%R) and (qt) for the effect of shaking time.

	Shake time	Percentage removal (% R)	Adsorption capacity (qt)mg/g
$V_2O_5.1.8H_2O$	10	55.55	4.68
	20	58.40	5.25
	30	56.19	4.89
	40	55.93	4.75
	50	52.88	4.28
	60	51.40	3.96
	70	50.98	3.74

Conclusion

The hydrothermal method (reflex) was successfully employed to produce the nanoparticles, which characterized using FTIR, UV-visible spectroscopy, XRD, SEM, and AFM. The results indicate that these nanoparticles are effective in removing AMX from solution samples. Among all these nanoparticles, vanadium pentoxide heated at 90 °C ($V_2O_5.1.8H_2O$) has the highest adsorption capacity (qt) to remove AMX from water, which arrived at 8.76 mg/g. While its annealing sample (V_2O_5) has the highest adsorption capacity (qt) to remove AMX from water, which arrived at 8.56 mg/g. Despite V_2O_5 nanoparticles having lower average grain size (21.49 nm) compared with the $V_2O_5.1.8H_2O$ sample (30.51 nm). The reason for that may be related to $V_2O_5.1.8H_2O$ nanoparticles having more oxygen and hydrogen to form hydrogen bonds with pollutants (AMX).

Acknowledgement

This work was supported by **Dr. Rashed T. Rasheed.** Thanks for the help provided to successfully complete this research/work.

References

[1] A. Al-Abduljabbar and I. Farooq, "Electrospun polymer nanofibers: Processing, properties, and applications," Polymers, vol. 15, no. 1, 2022, doi: 10.3390/polym15010065.

[2] S. Al-Asheh and A. Aidan, "A comprehensive method of ion exchange resins regeneration and its optimization for water treatment," in Promising Techniques for Wastewater Treatment and Water Quality Assessment, IntechOpen, 2021, doi: 10.5772/intechopen.93429.

[3] İ. M. Alkaç, B. Çerçi, C. Timuralp, and F. Şen, "Nanomaterials and their classification," in Nanomaterials for Direct Alcohol Fuel Cells, Elsevier, 2021, pp. 17–33, doi: 10.1016/B978-0-12-821713-9.00011-1.

[4] B. H. Alshammari et al., "Organic and inorganic nanomaterials: Fabrication, properties and applications," RSC Advances, vol. 13, no. 20, pp. 13735–13785, 2023, doi: 10.1039/D3RA01421E.

[5] Y. Amangelsin, Y. Semenova, M. Dadar, M. Aljofan, and G. Bjørklund, "The impact of tetracycline pollution on the aquatic environment and removal strategies," Antibiotics (Basel), vol. 12, no. 3, 2023, doi: 10.3390/antibiotics12030440.

[6] Aqel, K. M. M. A. El-Nour, R. A. A. Ammar, and A. Al-Warthan, "Carbon nanotubes, science and technology part (I): Structure, synthesis and characterisation," Arabian Journal of Chemistry, vol. 5, no. 1, pp. 1–23, 2012, doi: 10.1016/j.arabjc.2010.08.022.

[7] Balakrishnan, M. Chinthala, R. K. Polagani, and D.-V. N. Vo, "Removal of tetracycline from wastewater using g-C_3N_4 based photocatalysts: A review," Environmental Research, vol. 216, Pt 3, p. 114660, 2023, doi: 10.1016/j.envres.2022.114660.

[8] M. Balali-Mood, K. Naseri, Z. Tahergorabi, M. R. Khazdair, and M. Sadeghi, "Toxic mechanisms of five heavy metals: Mercury, lead, chromium, cadmium, and arsenic," Frontiers in Pharmacology, vol. 12, p. 643972, 2021, doi: 10.3389/fphar.2021.643972.

[9] V. Balaram, L. Copia, U. S. Kumar, J. Miller, and S. Chidambaram, "Pollution of water resources and application of ICP-MS techniques for monitoring and management—A comprehensive review," Geosystems and Geoenvironment, vol. 2, no. 4, p. 100210, 2023, doi: 10.1016/j.geogeo.2023.100210.

[10] Barhoum et al., "Review on natural, incidental, bioinspired, and engineered nanomaterials: History, definitions, classifications, synthesis, properties, market, toxicities, risks, and regulations," Nanomaterials (Basel, Switzerland), vol. 12, no. 2, p. 177, 2022, doi: 10.3390/nano12020177.

[11] "Bioinspired, and Engineered Nanomaterials: History, Definitions, Classifications, Synthesis, Properties, Market, Toxicities, Risks, and Regulations," Nanomaterials (Basel, Switzerland), vol. 12, no. 2, p. 177, 2022, doi: 10.3390/nano12020177.

[12] S. Bayda, M. Adeel, T. Tuccinardi, M. Cordani, and F. Rizzolio, "The history of nanoscience and nanotechnology: From chemical-physical applications to nanomedicine," Molecules, vol. 25, no. 1, p. 112, 2019, doi: 10.3390/molecules25010112.

[13] P. Bhatt, C.-H. Jeon, and W. Kim, "Tetracycline bioremediation using the novel Serratia marcescens strain WW1 isolated from a wastewater treatment plant," Chemosphere, vol. 298, p. 134344, 2022, doi: 10.1016/j.chemosphere.2022.134344.

[14] D. Bokov et al., "Nanomaterial by sol-gel method: Synthesis and application," Advances in Materials Science and Engineering, vol. 2021, p. 5102014, 2021, doi: 10.1155/2021/5102014.

[15] J. Briffa, E. Sinagra, and R. Blundell, "Heavy metal pollution in the environment and their toxicological effects on humans," Heliyon, vol. 6, no. 9, p. e04691, 2020, doi: 10.1016/j.heliyon.2020.e04691.

[16] V. Burke et al., "Occurrence of antibiotics in surface and groundwater of a drinking water catchment area in Germany," Water Environment Research, vol. 88, no. 7, pp. 652–659, 2016, doi: 10.2175/106143016X14609975746604.

[17] F. C. Cabello et al., "Antimicrobial use in aquaculture re-examined: Its relevance to antimicrobial resistance and to animal and human health," Environmental Microbiology, vol. 15, no. 7, pp. 1917–1942, 2023, doi: 10.1111/1462-2920.12134.

[18] Chahal et al., "Pathogen and particle associations in wastewater: Significance and implications for treatment and disinfection processes," Advances in Applied Microbiology, vol. 97, pp. 63–119, 2016, doi: 10.1016/bs.aambs.2016.08.001.

[19] Chen, Y. Chen, C. Ding, H. Liang, and B. Yang, "Effects of tetracycline on simultaneous biological wastewater nitrogen and phosphorus removal," RSC Advances, vol. 5, no. 73, pp. 59326–59334, 2015, doi: 10.1039/C5RA08434B.

[20] W.-R. Chen and C.-H. Huang, "Transformation kinetics and pathways of tetracycline antibiotics with manganese oxide," Environmental Pollution, vol. 159, no. 5, pp. 1092–1100, 2011, doi: 10.1016/j.envpol.2011.02.027.

[21] R. Daghrir and P. Drogui, "Tetracycline antibiotics in the environment: A review," Environmental Chemistry Letters, vol. 11, no. 3, pp. 209–227, 2013, doi: 10.1007/s10311-013-0404-8.

[22] S. Dai, Y. Ma, and K. Zhang, "Land degradation caused by construction activity: Investigation, cause and control measures," International Journal of Environmental Research and Public Health, vol. 19, no. 23, p. 16046, 2020, doi: 10.3390/ijerph192316046.